Materials Science and Engineering A 398 (2005) 37–46

www.elsevier.com/locate/msea

Effect of hydrogen and stress concentration on the notch tensile strength of AISI 4135 steel

Maoqiu Wang *,[1], Eiji Akiyama **, Kaneaki Tsuzaki

Steel Research Center, National Institute for Materials Science, Tsukuba, Ibaraki 305-0047, Japan

Received 11 November 2004; received in revised form 9 February 2005; accepted 4 March 2005

Abstract

The quantitative relationship between notch tensile strength and diffusible hydrogen content has been investigated for the AISI 4135 steel at 1320 MPa. The notch tensile strength was obtained by means of a slow strain rate test on circumferentially notched round bar specimens with stress concentration factors of 2.1, 3.3 and 4.9 after hydrogen charging, and the diffusible hydrogen content was then measured by thermal desorption spectrometry analysis. The diffusible hydrogen has been found to decrease the notch tensile strength in a power law manner, and the decrease is more prominent at a higher stress concentration factor. The finite element analysis results of stress and hydrogen distributions in the vicinity of the notch root have shown that the local fracture stress decreases with increasing local hydrogen concentration as the diffusible hydrogen content or stress concentration factor increases, resulting in the decrease in the notch tensile strength.
© 2005 Elsevier B.V. All rights reserved.

Keywords: Hydrogen embrittlement; Martensitic steels; Hydrogen desorption; Slow strain rate test (SSRT); Finite element analysis (FEA)

1. Introduction

Hydrogen embrittlement of high strength steels has been investigated extensively [1–5]; however, the quantitative relationship between hydrogen content and hydrogen embrittlement susceptibility, which is usually characterized by the losses of ductility, strength and toughness, has hardly been reported [6]. It may be difficult to obtain this relationship because high strength steels may exhibit high hydrogen embrittlement susceptibility at very low hydrogen contents, at even less than 1 mass ppm. In most cases, hydrogen embrittlement susceptibility was indirectly correlated with electrochemical charging conditions [7] or hydrogen gas pressure [8]. Recently, Endos and Scully have found a logarithmic relationship between the notch tensile strength and diffusible hydrogen content for a high strength pearlitic steel [9]. Zakroczymski et al. investigated the effect of hydrogen concentration on the embrittlement of a duplex stainless steel and found a linear correlation between the logarithm of the loss of ductility and the logarithm of hydrogen content [10]. Our recent research on a boron-bearing martensitic steel at 1050 and 1300 MPa also showed a power law relationship between the notch tensile strength and diffusible hydrogen content when hydrogen-induced intergranular fracture occurred [11]. Thus, a direct correlation of hydrogen embrittlement susceptibility and hydrogen content still needs to be examined.

On the other hand, notched specimens were commonly used in the study of hydrogen embrittlement, but the effect of stress concentration factor on hydrogen embrittlement did not attract much interest. Steinman et al. [12] once compared the susceptibilities of the cylindrical specimens with sharp and blunt notches when they investigated the hydrogen embrittlement of quenched and tempered AISI 4140 steel. They concluded that the effect of hydrogen increases with notch severity. Later Walter and Chandler studied the effect of notch severity on the embrittlement of low alloy steels and found that the reduction in notch strength of the low alloy steels increased with stress concentration factor (K_t) at low K_t values, reaching a maximum for $K_t = 6$–9, and then decreasing with K_t for higher K_t values [13]. Recently,

* Corresponding author. Tel.: +81 298 59 2131; fax: +81 298 59 2101.
** Co-corresponding author. Tel.: +81 298 59 2122; fax: +81 298 59 2101.
E-mail addresses: wang.manoqiu@nims.go.jp (M. Wang), akiyama.eiji@nims.go.jp (E. Akiyama).
[1] On leave from the Central Iron and Steel Research Institute, Beijing, PR China.

0921-5093/$ – see front matter © 2005 Elsevier B.V. All rights reserved.
doi:10.1016/j.msea.2005.03.008

Hardie and Liu investigated the effect of stress concentration on hydrogen embrittlement of the AISI 4340 steel and also concluded that increasing stress concentration makes hydrogen more effective as an embrittlement agent [14]. Although they found higher hydrogen embrittlement susceptibility in the specimens with higher notch severity, little effort was made to correlate hydrogen concentration and local fracture stress in the vicinity of the notch root to understand the underlying mechanism of the stress concentration effect.

In fact, it is difficult to measure hydrogen concentration in the vicinity of the notch root, although several experimental methods such as secondary ion mass spectroscopy (SIMS) [15] and hydrogen microprint technique (HMT) [16] have been used recently to observe hydrogen distribution. Accordingly, a numerical method has been used as a substitute to simulate hydrogen distribution by taking the hydrogen trapping effect into account for some cases [17–19]. With regard to hydrogen transport by dislocation movement and stress-driven diffusion, it has been proved by numerical simulation that hydrogen distribution in high strength steels is probably dominated by hydrostatic stress [20]. Thus, it is possible to correlate hydrogen concentration and local fracture stress with the help of a numerical method in the vicinity of the notch root.

The purpose of the present study is to investigate the quantitative relationship between the notch tensile strength and diffusible hydrogen content of quenched and tempered AISI 4135 steel at 1320 MPa. The hydrogen effect on the notch tensile strength of the specimens with different stress concentration factors has been studied. The hydrogen and stress distributions in the vicinity of the notch root are also calculated by the finite element analysis (FEA) to understand the effect of the stress concentration factor.

2. Experimental

2.1. Material and specimens

A commercial purity melt of an AISI 4135 steel was used in the present study, with the chemical composition listed in Table 1. Hot-rolled bars with a diameter of 22 mm were austenitized at 1133 K for 1 h, quenched into oil, and then tempered at 733 K for 1.5 h. Tensile tests were carried out at a strain rate of $4 \times 10^{-4}\ s^{-1}$ on the specimens with a diameter of 3.5 mm and a gauge length of 17.5 mm, machined from the heat-treated bars. The circumferentially notched round bar specimens with a notch root radius of $\rho = 0.1$, 0.25 or 0.8 mm, shown in Fig. 1, were also machined from the heat-treated bars and used for the slow strain rate test (SSRT). The calculated stress concentration factors for the specimens with notch root radii of 0.1, 0.25 and 0.8 mm were 4.9, 3.3 and 2.1, respectively [21].

Table 1
Chemical composition of the steel investigated (mass%)

C	0.35
Si	0.19
Mn	0.79
P	0.019
S	0.014
Cr	1.16
Mo	0.16
Cu	0.17
Fe	Balance

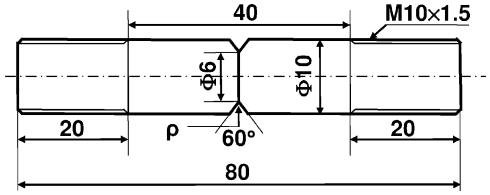

Fig. 1. Dimensions (in mm) of the notched round bar specimens for the SSRT, where the notch root radius (ρ) is 0.1, 0.25 or 0.8 mm for the K_t = 4.9, 3.3 or 2.1 specimen.

2.2. Hydrogen charging and homogenizing

Hydrogen was introduced into the specimens by electrochemical charging in either 3% NaCl + 0.3% NH_4SCN or 0.1N NaOH aqueous solution at the current density of 0.3–30 A/m^2 for 48 or 72 h. There was no evidence of surface damage or cracking even after charging at the highest applied current density of 30 A/m^2. Following hydrogen charging, the specimens were mechanically polished with #1000 SiC grit paper and then electroplated with a cadmium coating of about 15 μm in thickness to prevent hydrogen release [22]. Then, the specimens that were charged for 48 h were kept at ambient temperature for 24 h before the SSRT to homogenize the hydrogen distribution in the specimens. Assuming that hydrogen entry during charging is only controlled by diffusion, theoretical calculations using the experimentally obtained hydrogen diffusion coefficient ($D = 3.8 \times 10^{-11}\ m^2/s$) in the steel [23] show that the difference in hydrogen distribution in the specimens is within ±5% after a total time of 72 h for charging and homogenizing. Thus, it is reasonable to assume that the hydrogen distribution in the specimens before the SSRT is homogeneous.

2.3. SSRT

SSRT was carried out on a Shimadzu AG-250kNI tensile testing machine with a constant crosshead speed of 0.005 mm/min, corresponding to a nominal strain rate of $8.3 \times 10^{-7}\ s^{-1}$. The duration of SSRT ranged from 1 to 5 h, depending on the fracture stress of the specimen. The notch tensile strength was defined as follows:

$$\sigma_{NB} = \frac{F_{max}}{A_{min}} \quad (1)$$

where F_{max} is the maximum tensile load and A_{min} is the initial cross-section net area of the notch. To prevent hydrogen release, the specimens were put into liquid nitrogen immediately after the SSRT and kept there until an electrochemical removal of the cadmium coating was made before the hydrogen measurement.

2.4. TDS analysis

The average hydrogen content in the specimen was measured by means of a thermal desorption spectrometry (TDS) analysis using a quadru-pole mass (Q-mass) spectrometer at a heating rate of 100 K/h. The TDS analyses were conducted from ambient temperature to 1073 K to obtain hydrogen desorption profiles. The total hydrogen desorbed at the first peak below 600 K was defined as diffusible hydrogen in the present study, which is so called because it can gradually diffuse out during the exposure of the specimen at ambient temperature. Several heating rates were also used for determining the activation energy of hydrogen desorption. The hydrogen escape rate from a trapping site was assumed as follows [24]:

$$\frac{dx}{dt} = A(1-x)e^{-E_a/RT} \quad (2)$$

where $x = (N_0 - N)/N_0$. N_0 and N are the amounts of hydrogen in the trapping site at $t = 0$ and >0, respectively. E_a is the activation energy, A the constant, T the absolute temperature and R is the gas constant ($R = 8.314$ J/mol K). At the hydrogen desorption peak, the escape rate reaches a maximum, and the derivative of the escape rate against time should be equal to zero. Then, the activation energy of hydrogen desorption can be calculated from the dependence of the peak temperatures on the heating rates according to the following equation [24]:

$$\frac{\partial \ln\left(\frac{\Phi}{T_p^2}\right)}{\partial\left(\frac{1}{T_p}\right)} = -\frac{E_a}{R} \quad (3)$$

where Φ is the heating rate and T_p is the peak temperature.

2.5. Microscopic observation

Optical observation was carried out by means of a standard metallographic method using a 2% initial as the etchant. Thin film samples were cut from the heat-treated bars, mechanically ground and polished to a thickness of about 0.08 mm, and then electrochemically thinned with a double jet polishing machine in a 5 vol% perchloric acid ($HClO_4$) and 95 vol% methanol (CH_3OH) solution at 243 K. A transmission electron microscope (TEM), JEOL 2000FX, operating at 200 kV, was used in this study. The fracture surfaces were observed on a JSM 5400 type scanning electron microscope (SEM), operating at 15 kV.

3. Theoretical models

3.1. Model for stress and strain distributions

The stress and strain distributions in the notched specimens were calculated by means of FEA using the commercial finite element modeling software ANSYS 5.7/Multiphysics 2. A two-dimensional axisymmetric model with eight-node elastic–plastic elements (PLANE 82) was used with a minimum mesh size of about 0.5 μm. Fine meshes were arranged in a region near the notch root, and the element numbers for the specimens with stress concentration factors of $K_t = 4.9$, 3.3 and 2.1 were 2376, 2376 and 2144, respectively. Only one-half of the geometry was analyzed due to symmetry. The true stress–true strain curve obtained by the tensile test mentioned above was used as the stress–strain response, and a power-hardening relation in the form of $\sigma = K\varepsilon^n$ was assumed for extrapolating the stress–strain curve to the high strain region where necking occurred during the tensile test. The influence of hydrogen on the stress–strain response was not taken into account in the present study because the tensile stress–strain curve of hydrogen charged smooth specimens did not show any clear difference from that of the uncharged specimen before necking, as shown in Fig. 2.

3.2. Model for hydrogen distribution

The maximum principal stress, hydrostatic stress and equivalent plastic strain were calculated at an applied stress up to the experimentally obtained notch tensile strength. As proved by numerical simulation, hydrogen distribution in high strength steels is dominated by hydrostatic stress even when the plastic strain is as high as 2.3% [20]. Therefore, by assuming an equilibrium state of hydrogen diffusion, the locally accumulated hydrogen concentration at a stress concentrated region can be calculated according to the following

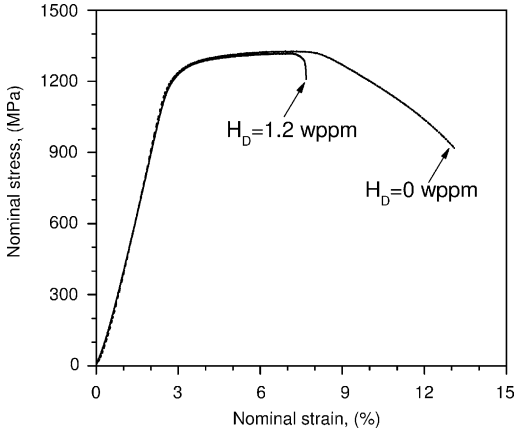

Fig. 2. Comparison of the nominal stress–nominal strain curves of the uncharged ($H_D = 0$ wppm) and hydrogen charged ($H_D = 1.2$ wppm) smooth specimens.

equation [25]:

$$H = H_D \exp\left[\frac{-V_H(\sigma_h - \sigma_{h,min})}{RT}\right] \quad (4)$$

where σ_h is the hydrostatic stress at the stress concentration region, $\sigma_{h,min}$ the hydrostatic stress in the region far from the notched section, V_H the partial molar volume of hydrogen in bcc-Fe ($V_H = 2.1 \times 10^{-6}$ m^3/mol) [26], R the gas constant, T the testing temperature ($T = 300$ K) and H_D is the diffusible hydrogen content in the specimen that could be measured by the TDS from the fractured specimens. If the amount of hydrogen in the specimen is time independent and the stress increases continuously with time, which occurs in the SSRT, the hydrogen concentration calculated from the above equation should be multiplied by a factor to keep the mass conservation law. This factor is calculated as follows:

$$f = \frac{H_D \sum_i V_i}{\sum_i (V_i H_i)} \quad (5)$$

where V_i is the volume of an element and H_i is the hydrogen concentration of an element that is calculated by Eq. (4).

4. Results and discussion

4.1. Microstructure and tensile properties

The tensile properties of the steel tempered at 733 K are shown in Table 2. The tempering resulted in both a high tensile strength and a good ductility for the steel. Fig. 3a shows that the steel had relatively fine prior austenite grains with a mean size of 11 μm. The tempered martensitic microstructure was obtained with fine carbides that precipitated within martensite laths and at the lath boundaries and the prior austenite grain boundaries. Fig. 3b shows rod-like M_3C type carbides from a TEM observation. The mean size of the carbides was approximately 150 nm in length and 40 nm in diameter. M_2C type carbides, which can act as reversible hydrogen trapping sites [27], were not found in the present steel since the usual precipitation temperature of M_2C carbides is above 773 K [28].

4.2. Hydrogen desorption and trapping

Typical hydrogen desorption curves of the steel are shown in Fig. 4. At a heating rate of 100 K/h, the uncharged specimen showed a small hydrogen desorption peak at 718 K and the measured hydrogen content corresponding to this peak was less than 0.01 wppm. Hydrogen charging resulted in an additional hydrogen desorption peak at around 423–453 K. The hydrogen corresponding to this low temperature peak can gradually diffuse out during the exposure of the specimen at ambient temperature and was observed in a similar steel of AISI 4140 by Kimura et al. [29]. Thus, it is regarded as diffusible hydrogen. Under the charging conditions used in the present study, a diffusible hydrogen content up to 2.5 wppm was charged for the steel.

Table 2
Tensile properties of the steel after 733 K tempering

UTS σ_B (MPa)	1320
YS $\sigma_{0.2}$ (MPa)	1235
Total El ε_t (%)	14
RA ψ (%)	56

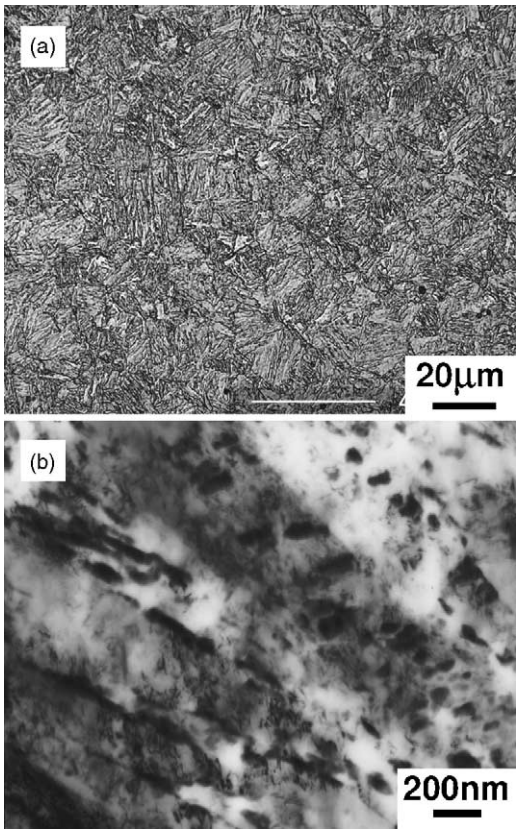

Fig. 3. Microstructure of the steel after 733 K tempering, (a) optical micrograph and (b) TEM bright-field micrograph.

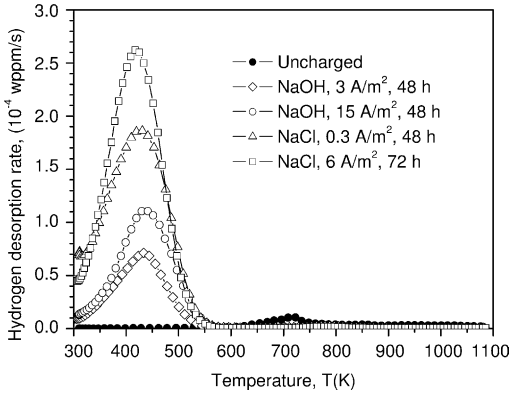

Fig. 4. Typical hydrogen desorption curves of the uncharged specimen and hydrogen charged specimens, NaOH and NaCl representing the two charging solutions followed by charging current density and charging time.

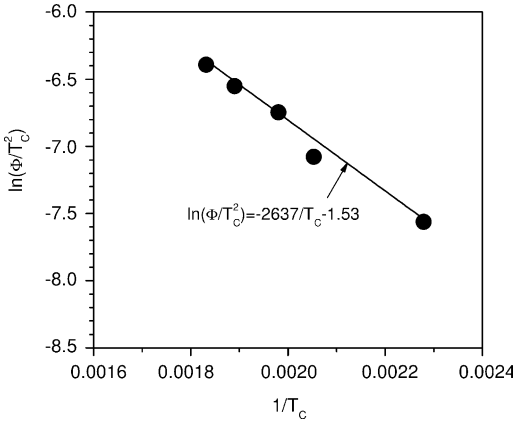

Fig. 5. Plot of the heating rate Φ and peak temperature T_c dependent parameter $\ln(\Phi/T_c^2)$ as a function of $1/T_c$ for determination of the activation energy of hydrogen desorption.

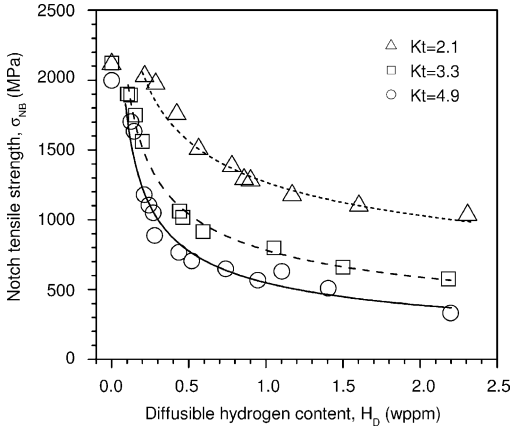

Fig. 6. Dependence of notch tensile strength on diffusible hydrogen content for the specimens with different stress concentration factors.

Fig. 5 shows the plot of $\ln(\Phi/T_c^2)$ against $(1/T_c)$ for the desorption peak corresponding to diffusible hydrogen. Thus, the activation energy of hydrogen desorption was calculated to be 21.9 kJ/mol from the slope of the linear regression line according to Eq. (3). Since the activation energy for hydrogen diffusion in the iron lattice was reported to be less than 10 kJ/mol [30], some of the hydrogen in the specimen was probably trapped by some reversible trapping sites. By changing the grain size and dislocation density of the pure iron, Choo and Lee observed the two hydrogen desorption peaks at 385 and 488 K with desorption activation energies of 17.2 and 26.8 kJ/mol, respectively [24]. They concluded that these peaks were attributed to hydrogen trapped by grain boundaries and dislocations since no other microstructural changes were involved. Yamasaki and Takahashi reported a hydrogen desorption peak at around 373 K with an activation energy of 21 kJ/mol in quenched and tempered martensitic steels, and they also attributed the peak to hydrogen trapped by dislocations and prior austenite grain boundaries [31]. Recently, an activation energy of 21.9 kJ/mol was also found corresponding to hydrogen trapped by dislocation and grain boundaries in a 0.05 C–0.22 Ti–2.0 Ni steel [32]. Based on these previous research results, some of the measured diffusible hydrogen in the present steel was probably trapped by grain boundaries and dislocations since the activation energy and peak temperature were very similar to the reported ones.

4.3. Notch tensile strength

The dependence of the notch tensile strength on diffusible hydrogen content for the steel with different K_t values is shown in Fig. 6. All the hydrogen charged specimens showed a lower notch tensile strength than that of the uncharged specimens ($H_D = 0$ wppm), indicating a hydrogen embrittlement of the steel. For example, the notch tensile strength of the $K_t = 4.9$ specimen was less than 500 MPa when the diffusible hydrogen content was around 2 wppm, showing a loss of about 1500 MPa compared to that of the uncharged specimen. There was an apparent decrease in the notch tensile strength with increasing diffusible hydrogen content in the present experimental range. The notch tensile strength decreased sharply in the low hydrogen content region and slowly in the relatively high hydrogen content region. This trend can be expressed by a power law relationship as follows:

$$\sigma_{NB} = 548 H_D^{-0.5} \quad \text{when } K_t = 4.9 \tag{6}$$

$$\sigma_{NB} = 783 H_D^{-0.41} \quad \text{when } K_t = 3.3 \tag{7}$$

$$\sigma_{NB} = 1269 H_D^{-0.3} \quad \text{when } K_t = 2.1 \tag{8}$$

where σ_{NB} is the notch tensile strength in MPa and H_D is the diffusible hydrogen content in wppm.

Fig. 6 also shows that there were no clear differences in the notch tensile strength among the uncharged specimens ($H_D = 0$ wppm) with stress concentration factors of $K_t = 2.1$, 3.3 and 4.9; however, the charged specimens showed a big difference in the notch tensile strength. At the same diffusible hydrogen content, the specimen with a higher stress concentration factor exhibited a lower notch tensile strength. For example, at the diffusible hydrogen content of 0.5 wppm, the notch tensile strength decreased from 1500 MPa for the $K_t = 2.1$ specimen to 1000 MPa for the $K_t = 3.3$ specimen and to about 700 MPa for the $K_t = 4.9$ specimen. Apparently, hydrogen embrittlement susceptibility of the steel increased with stress concentration factor, indicating that increasing stress concentration makes hydrogen more effective as an embrittlement agent. This is due to the additional intensive stress concentration and hydrogen accumulation and will be discussed later.

4.4. Fractography

Fig. 7 shows the fracture surfaces of the uncharged specimens with $K_t = 4.9$ and 2.1. The uncharged specimens exhibited a fracture mode of microvoid coalescence (Fig. 7b and d), although the $K_t = 2.1$ specimen showed a relatively broad shear lip region near the notch root, indicating that in this case

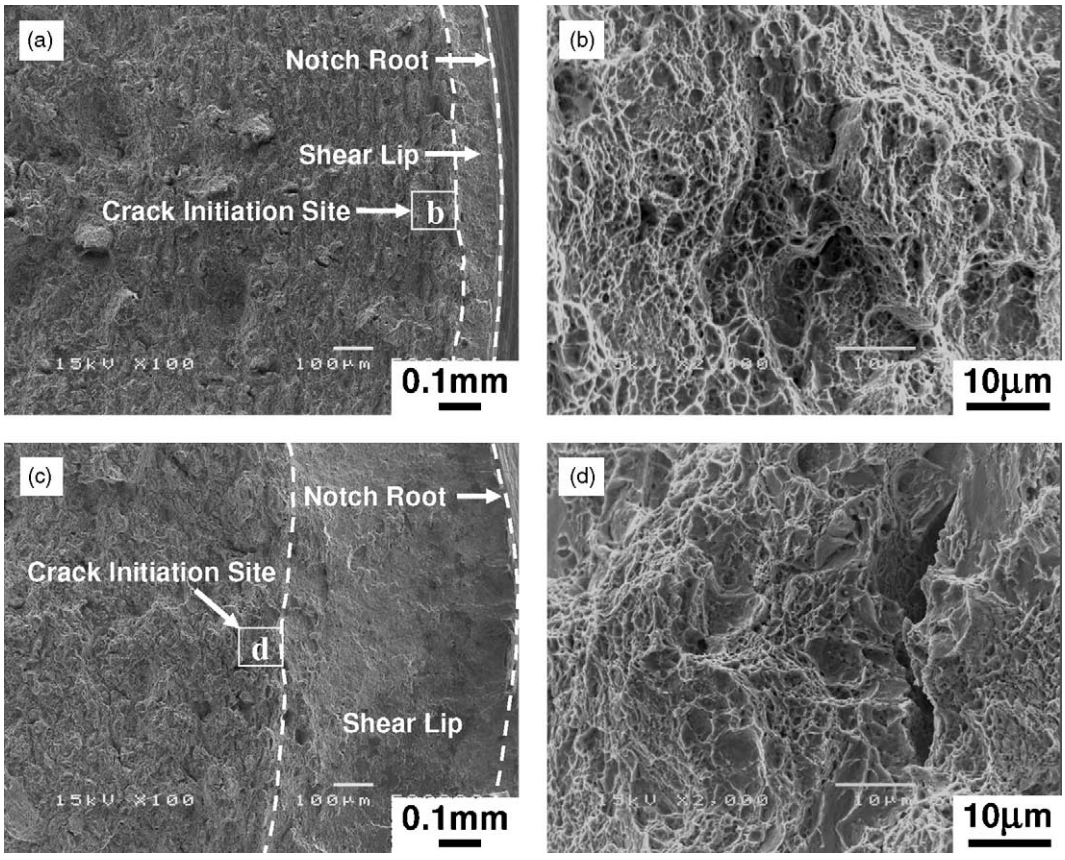

Fig. 7. SEM fractographs of the uncharged specimens with different stress concentration factors (K_t): (a) and (b) $K_t = 4.9$; and (c) and (d) $K_t = 2.1$; (b) and (d) high magnification images of the region near crack initiation site.

the crack initiation site is not in the vicinity of the notch root, but farther inside (Fig. 7c). The fracture surfaces of the hydrogen charged specimens with different stress concentration factors and different diffusible hydrogen contents are shown in Figs. 8 and 9 at lower and higher magnifications, respectively. Compared to the uncharged specimens, the hydrogen charged specimens exhibited a brittle intergranular (IG) fracture appearance in the vicinity of the crack initiation site, as indicated by the IG regions in Figs. 8 and 9. The area fraction of IG fracture increased with diffusible hydrogen content and stress concentration factor, indicating the embrittlement effect of hydrogen and stress concentration. As can be seen in Fig. 9a and b for the $K_t = 3.3$ specimens, the IG area as well as the crack initiation site was located closer to the notch root when the diffusible hydrogen concentration was higher. A shear lip region could also be observed around the notch root on the hydrogen charged specimens, especially with a lower stress concentration factor. Apparently, the area fraction of the shear lip region increased with decreasing stress concentration factor. The magnified views of the IG fracture region and the shear lip region are shown in Fig. 9c and d, respectively. The fracture surfaces were consistent with the notch tensile strength, and a higher loss in notch tensile strength was usually associated with a more brittle fracture appearance.

4.5. Stress, strain and hydrogen distributions

Fig. 10 shows the calculation results of the distribution of the maximum principal stress, equivalent plastic strain and hydrogen concentration for the specimens with a diffusible hydrogen content of 1 wppm. The applied net stresses were calculated from Eqs. (6–8) by assuming $H_D = 1$ wppm, being 548, 783 and 1269 MPa for the $K_t = 4.9$, 3.3 and 2.1 specimens, respectively. As the K_t value increased, the distributions of the maximum principal stress, equivalent plastic stress and hydrogen concentration became sharper. Furthermore, the distributions of the maximum principal stress and hydrogen concentration had a peak, which was located farther inside the notch root for the specimen with a lower stress concentration factor, while the maximum equivalent plastic strain always occurred on the notch root surface. All the calculated diffusible hydrogen concentrations were higher than 1 wppm in the radial direction in the vicinity of the notch root due to hydrogen diffusion from the other parts of the specimen.

The stress and strain distributions can account for the fracture surfaces of the hydrogen charged specimens. For the specimens with a lower stress concentration factor, the IG fracture was found farther away from the notch root, and a shear lip region was observed in the vicinity of the notch root.

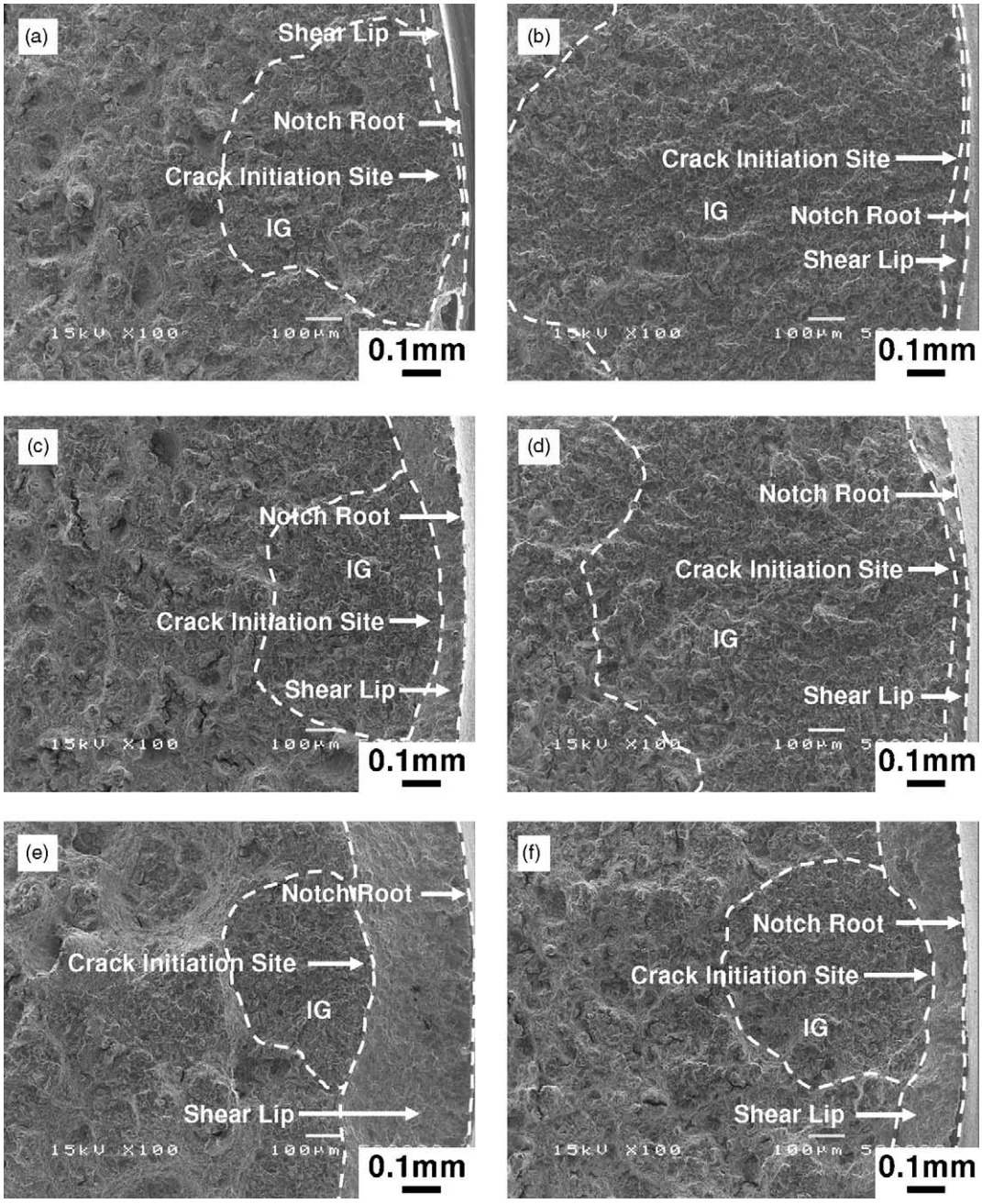

Fig. 8. SEM fractographs of the hydrogen charged specimens with different stress concentration factors (K_t) and diffusible hydrogen contents (H_D): (a) and (b) $K_t = 4.9$; (c) and (d) $K_t = 3.3$; and (e) and (f) $K_t = 2.1$; (a), (c) and (e) $H_D = 0.4$ wppm, and (b), (d) and (f) $H_D = 1$ wppm.

The shear lip region occurred as a result of high plastic strain, and the IG fracture seemed to be related to the stress peak. Decreasing stress concentration factor results in a flatter strain distribution in the vicinity of the notch root, providing high plastic strain at a longer distance than the shear lip requires. The stress peak also moves farther inside with decreasing stress concentration factor, which is consistent with the movement of the IG fracture, indicating that the peak stress, which is also regarded as a local fracture stress, seems to play an important role in the hydrogen embrittlement process of the steel.

4.6. Local fracture stress and local hydrogen concentration

Fig. 11 shows the plot of the peak value of the maximum principal stress (σ_p^*) as a function of the peak value of the locally accumulated diffusible hydrogen concentration (H_D^*) for the specimens with various stress concentration factors and diffusible hydrogen contents. Despite the difference in the stress concentration factor, all the data points were in good agreement with a power law relationship within experimental scatter as follows:

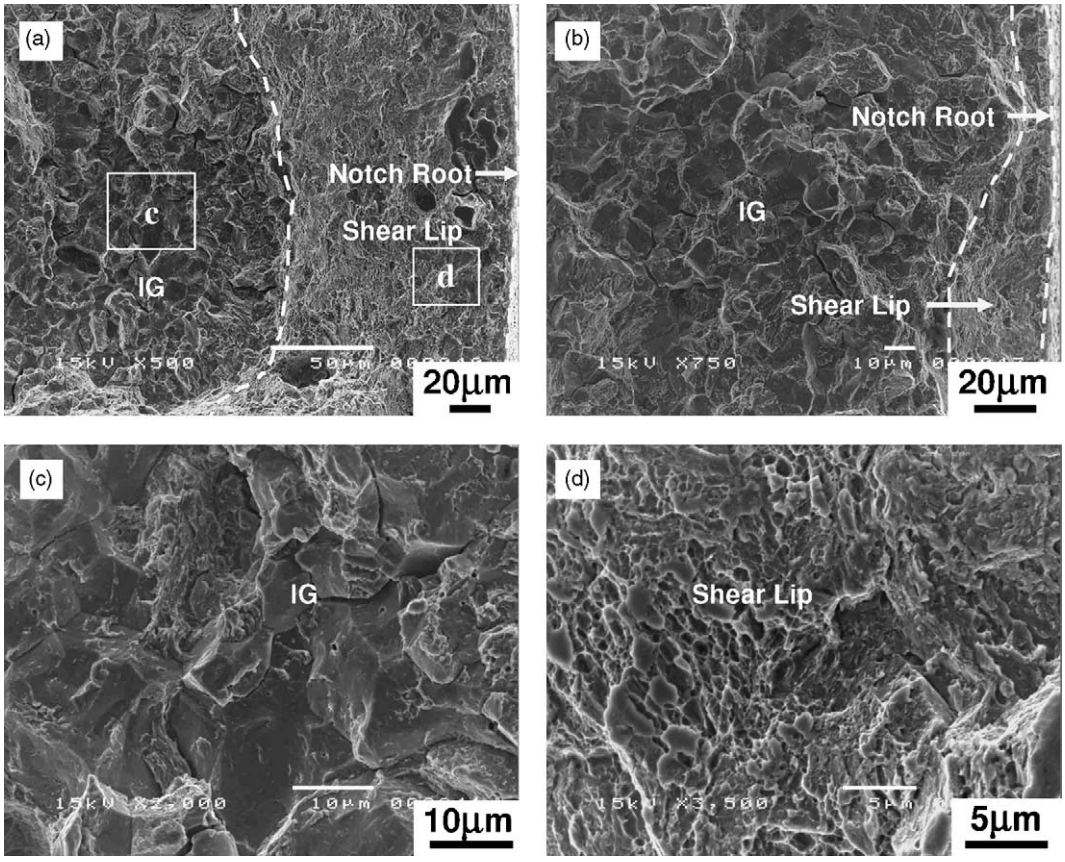

Fig. 9. Higher magnification images of the $K_t = 3.3$ specimen with the diffusible hydrogen contents of 0.4 wppm (a, c and d) and 1 wppm (b) showing the regions of (a) and (b) the vicinity of the notch root, (c) IG fracture and (d) shear lip.

$$\sigma_p^* = 2108 H_D^{*-0.23} \tag{9}$$

It implies that hydrogen embrittlement of the steel is controlled by local stress and local hydrogen concentration and only occurs when the critical combination of local stress and local hydrogen concentration is satisfied.

Since the specimens with different stress concentration factors showed a unitive σ_p^* versus H_D^* relationship, Eq. (9) can be regarded as a fracture criterion for the hydrogen embrittlement of the AISI 4135 steel. Some criteria which emphasize the important role of plastic strain in hydrogen embrittlement were previously proposed [33–35]. For high strength pearlitic steels, Toribio and Elices once formulated a fracture criterion, which considers that the fracture takes place when the distortional part of the strain energy density reaches a critical value over a critical region [33,34]. However, the fracture criterion cannot be readily used for the present AISI 4135 steel since the critical region was correlated with the fracture surfaces of the so-called topography tearing surface (TTS), which was different from the IG fracture surfaces that were observed for the present steel. Another criterion was proposed by Wall et al. to characterize the brittle fracture of the 9Cr1Mo steel, by considering the brittle fracture to be a dynamic event occurring at an intermediate position between the notch root and the peak stress [35]. Although the criterion is theoretically reasonable, it is not easy to find the exact crack initiation site, so it cannot be used readily.

The hydrogen embrittlement of the AISI 4135 steel is locally stress-controlled, thus the effect of hydrogen is to reduce the cohesive strength. With regard to the effect of hydrogen on cohesive strength, a linear decrease in the critical maximum local tensile stress was often assumed with increasing hydrogen content [36–38]. A square root relationship was also suggested from the experimental results on the segregation reduced grain boundary strength as follows [39,40]:

$$\sigma^* = \sigma_0^* - aC_H^{1/2} \tag{10}$$

where σ^* and C_H are the critical value of the maximum local tensile stress and the hydrogen concentration at the fracture site, respectively. σ_0^* and a are the two constants, the former being the critical value of the maximum local tensile stress in the absence of hydrogen. However, a power law existed between the local fracture stress and local diffusible hydrogen concentration for the present steel indicating that the hydrogen decreases the cohesive strength of the AISI 4135 steel in a power law manner, which in return decreases the notch tensile strength in a power law manner.

Finally, the effect of stress concentration on the notch tensile strength can be attributed to hydrogen accumulation as

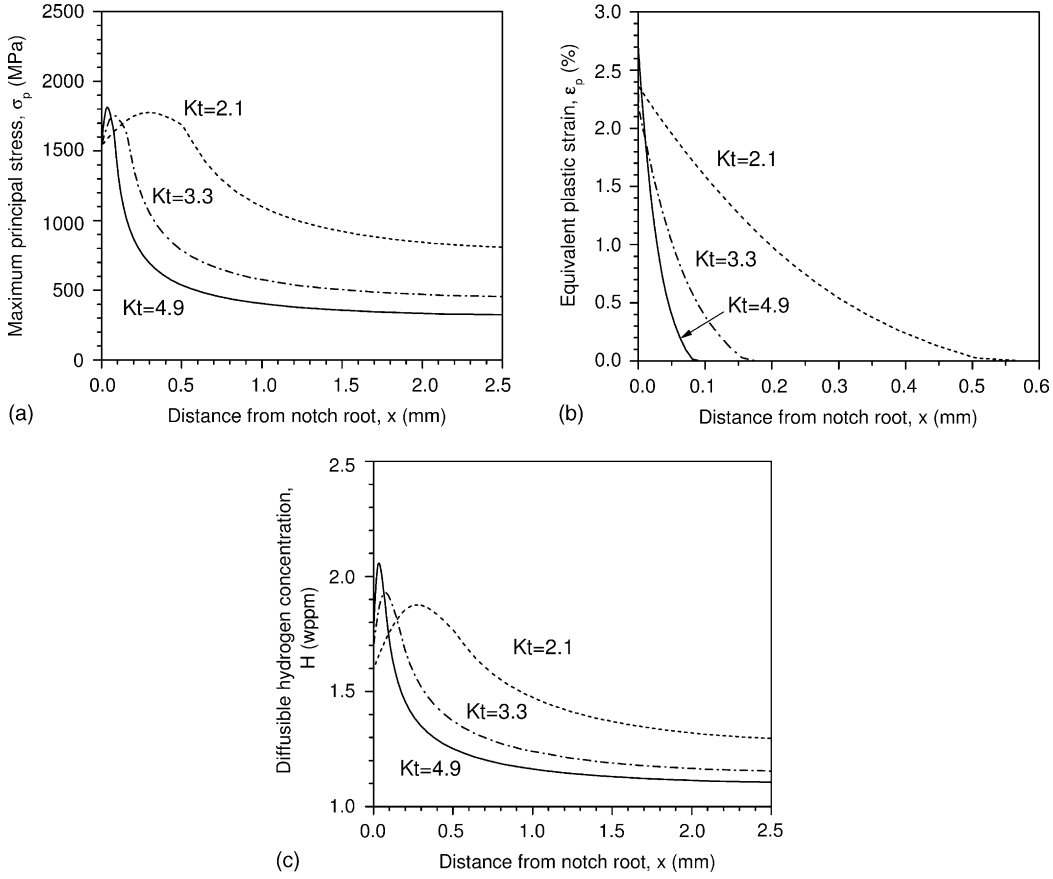

Fig. 10. FEA calculation results on the distributions of (a) maximum principal stress, (b) equivalent plastic strain and (c) diffusible hydrogen concentration in the radial direction near the notch root for the specimens with a diffusible hydrogen content of 1 wppm.

well as to increased local peak stress. At the same diffusible hydrogen content, the notch tensile strength increases with decreasing stress concentration factor because a higher local fracture stress is needed for the specimens with a lower stress concentration factor with less intensive hydrogen accumulation.

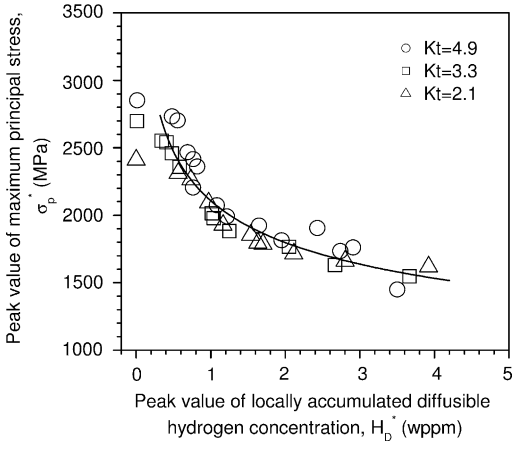

Fig. 11. Plot of the peak value of maximum principal stress and the peak value of locally accumulated diffusible hydrogen concentration for the specimens with different stress concentration factors.

5. Conclusions

Hydrogen embrittlement of quenched and tempered AISI 4135 steel at 1320 MPa was investigated by means of a SSRT using circumferentially notched round bar specimens with stress concentration factors of $K_t = 4.9$, 3.3 and 2.1. To understand the effect of stress concentration factor on the notch tensile strength, FEA calculations were carried out to simulate stress, strain and hydrogen distributions in the vicinity of the notch root. The following conclusions can be drawn:

(1) TDS analysis of the steel after hydrogen charging showed a hydrogen desorption peak at 423–453 K with an activation energy of 21.9 kJ/mol, corresponding to the hydrogen in lattice or trapped by reversible trapping sites such as grain boundaries and dislocations.
(2) Hydrogen decreased the notch tensile strength in a power law manner, and the effect was more prominent for the specimens with a higher stress concentration factor due to more intensive stress concentration and hydrogen accumulation.
(3) IG fracture was found in the hydrogen charged specimens while the uncharged specimens showed a ductile fracture mode. With decreasing hydrogen content or stress concentration factor, the IG fracture region moved farther

away from the notch root. A shear lip was found in the specimens with a lower stress concentration factor. The fracture surfaces can be accounted for by the stress and strain distributions in the vicinity of the notch root.

(4) FEA calculation results showed that the peak value of the maximum principal stress and the peak value of the locally accumulated diffusible hydrogen concentration were in good agreement with the power law relation for the specimens with different stress concentration factors. Hydrogen embrittlement of the steel was thus controlled by local stress and local hydrogen concentration.

(5) The local fracture stress and local hydrogen concentration can account for the effect of hydrogen and the stress concentration factor on the notch tensile strength of the steel.

Acknowledgements

The authors would like to acknowledge Mr. S. Terasaki of Ishikawajima-Harima Heavy Industries Co. Ltd. and Dr. K. Enami of National Institute for Materials Science for helpful discussions.

References

[1] A.R. Troiano, Trans. ASME 52 (1960) 54–80.
[2] I.M. Bernstein, Mater. Sci. Eng. 6 (1970) 1–19.
[3] J.P. Hirth, Metall. Trans. A 11A (1980) 861–890.
[4] S.P. Lynch, Acta Metall. 36 (1986) 2639–2661.
[5] M. Nagumo, Mater. Sci. Tech. 20 (2004) 940–950.
[6] A.W. Thompson, Mater. Sci. Tech. 1 (1985) 711–718.
[7] O.A. Onyewuenyi, J.P. Hirth, Metall. Trans. A 14A (1983) 259–269.
[8] W. Hofmann, W. Rauls, Weld. J. Res. Suppl. 44 (1965) 225s–230s.
[9] D.G. Endos, J.R. Scully, Metall. Mater. Trans. A 33A (2002) 1151–1166.
[10] T. Zakroczymski, A. Glowacka, W. Swiatnicki, Corros. Sci. 47 (2005) 1403–1414.
[11] M.Q. Wang, E. Akiyama, K. Tsuzaki, Scripta Mater. 52 (2005) 403–408.
[12] J.B. Steinman, H.C. Van Ness, G.S. Ansell, Weld. J. Res. Suppl. 44 (1965) 221s–224s.
[13] R.J. Walter, W.T. Chandler, Mater. Sci. Eng. 8 (1971) 90–97.
[14] D. Hardie, S.E. Liu, Corros. Sci. 38 (1996) 721–733.
[15] K. Takai, Y. Chiba, K. Noguchi, A. Nozue, Metall. Mater. Trans. A 33A (2002) 2659–2665.
[16] A. Nagao, S. Kuramoto, K. Ichitani, M. Kanno, Scripta Mater. 45 (2001) 1227–1232.
[17] C.A. Hippsley, C.L. Briant, Scripta Met. 19 (1985) 1203–1208.
[18] P. Sofronis, R.M. McMeeking, J. Mech. Phys. Solids 37 (1989) 317–350.
[19] A.T. Yokobori Jr., Y. Chinda, T. Nemoto, K. Satoh, T. Yamada, Corros. Sci. 44 (2002) 407–424.
[20] J. Lufrano, P. Sofronis, Acta Metall. 46 (1998) 1519–1526.
[21] S. Takagi, T. Inoue, K. Tsuzaki, F. Minami, J. Jpn. Inst. Met. 65 (2001) 1073–1081.
[22] H.H. Johnson, J.G. Morlet, A.R. Troiano, Trans. Metall. Soc. AIME 212 (1958) 528–536.
[23] S. Sakashita, E. Akiyama, K. Tsuzaki, T. Takahashi, CAMP-ISIJ 15 (2002) 576.
[24] W.Y. Choo, J.Y. Lee, Metall. Trans. A 13A (1982) 135–140.
[25] J.C.M. Li, R.A. Oriani, L.W. Darken, Z. Phys. Chem. 49 (1966) 271–290.
[26] H. Wagonblast, H.A. Wriedt, Metall. Trans. 2 (1971) 1393–1397.
[27] D.M. Li, R.P. Gangloff, J.R. Scully, Metall. Mater. Trans. A 35A (2004) 849–864.
[28] K. Kuo, J. Iron Steel Inst. (1956) 258–268.
[29] Y. Kimura, Y. Sakai, T. Hara, A. Belyakov, K. Tsuzaki, Scripta Mater. 49 (2003) 1111–1116.
[30] K. Kiuchi, R.B. McLellan, Acta Metall. 31 (1983) 961–984.
[31] S. Yamasaki, T. Takahashi, Tetsu-to-Hagané 83 (1997) 454–459.
[32] E.G. Wei, T. Hara, K. Tsuzaki, Metall. Mater. Trans. B 35B (2004) 587–597.
[33] J. Toribio, M. Elices, Corros. Sci. 33 (1992) 1387–1409.
[34] J. Toribio, Eng. Fract. Mech. 57 (1997) 391–404.
[35] M. Wall, C.E. Lane, C.A. Hippsley, Acta Metall. Mater. 42 (1994) 1295–1309.
[36] R.A. Oriani, P.H. Josephic, Acta Metall. 22 (1974) 1065–1074.
[37] K.N. Akhurst, T.J. Baker, Metall. Trans. A 12A (1981) 1059–1070.
[38] T. Zhang, W.Y. Chu, K.W. Gao, L.J. Qiao, Mater. Sci. Eng. A347 (2003) 291–299.
[39] S.V. Vair, J.K. Tien, Metall. Trans. A 16A (1985) 2333–2340.
[40] J. Kameda, C.J. McMahon Jr., Metall. Trans. A 14A (1983) 903–911.